Photochemistry and Photobiology, 2010, 86: 182–193

Distribution of Chlorophyll- and Bacteriochlorophyll-derived Photosensitizers in Human Blood Plasma

Jörg Dandler, Brigitte Wilhelm and Hugo Scheer*

Department Biologie I — Botanik, Universität München, Munich, Germany

Received 23 May 2009, accepted 18 July 2009, DOI: 10.1111/j.1751-1097.2009.00621.x

ABSTRACT

Chlorophyll *a* and, in particular, bacteriochlorophyll *a* derivatives are promising candidates for photosensitizers in photodynamic therapy. The distribution of 21 (bacterio)chlorophyll derivatives among human blood plasma fractions was studied by iodixanol gradient ultracentrifugation and *in situ* absorption spectroscopy. Modifications of the natural pigments involved the central metal (Mg^{2+}, Zn^{2+}, Pd^{2+}, none), the isocyclic ring (closed, open and taurinated), substituents at C-3 (vinyl, acetyl, 1-hydroxyethyl) and C-17^3 (phytyl ester, free acid). Cellular blood components bound only a small fraction of the pigments. Distribution among low-density lipoproteins (LDL), high-density lipoproteins (HDL) and high-density proteins (HDP) of the plasma was influenced as follows: (1) application in Cremophor® EL slightly altered pigment distribution by lipoprotein modification, (2) only very polar pigments with multiple hydrophilic substituents showed substantial HDP binding, (3) the presence of the esterifying alcohol at C-17^3 caused enrichment in LDL, this was more pronounced with bacteriochlorophylls than with chlorophylls, (4) substituents at C-3 had only little influence on the distribution, (5) Zn^{2+}-complexes were enriched in HDL compared to Mg^{2+} and Pd^{2+} complexes, indicating specific binding of the former. Equilibration of pigments among the different fractions was largely complete within 3 h.

INTRODUCTION

Photodynamic therapy (PDT) uses reactive oxygen species (ROS) to treat malignancies including cancer. ROS are generated by irradiating photosensitizing dyes by visible or near-infrared (NIR) light. Topical action of the generally intravenously injected photosensitizers is achieved by two factors. The first one involves concentration differences between healthy and transformed tissues, which were noted early (1,2) but whose origin is still only partly understood (3–6). The second factor is a spatially controlled irradiation of the transformed tissue (7,8). The strategy and details of the treatment protocols depend, among other factors, on the dynamics of pigment transport, its uptake and excretion, which in turn depend on the structure of the photosensitizer and its mode of injection. Protocols differ, for example, between slowly excreted pigments like hematoporphyrin derivative (HpD), and more rapidly excreted pigments. Examples of the latter type are chlorophyll (Chl) and bacteriochlorophyll (BChl) derivatives (9–17). These pigments absorb intensely in the red (Chls) and NIR spectral regions (BChls) where tissue is relatively transparent to light (18). Their rapid clearance is probably due to a combination of factors including an active excretion system (19,20), the photolability of many such derivatives (21–23) and possibly also to dark degradations by oxidative ring opening (24,25). The pharmacokinetics of these photosensitizers is therefore of considerable practical interest, but little is known so far on how this depends on the pigments' structures.

Details of the treatment will also depend on the intended target. While originally a cellular action had been assumed that involves ROS-initiated necrosis (26), more indirect actions have subsequently been suggested, including apoptotic signaling by ROS and a vascular action (6,27–33). Due to their rapid turnover times, (B)Chl derivatives are particularly suited for vascular targeting (34,35). Although the concept of such an indirect action has been emphasized increasingly during recent years, its translation into rational protocols is still difficult. It has also been recognized that the ROS generated by these pigments depend on their microenvironment (36,37). As a contribution to a rational approach, we present here a study on the partitioning of (B)Chl derivatives among the different fractions of human blood plasma (BP), its dependence on the structure of the pigments and the time required for equilibration. The pigments investigated range from the highly hydrophobic (B)Chls that are esterified by the diterpenoid alcohol, phytol, to the water-soluble taurinated BChl derivative, WST11, and HpD as a control. Almost all BChl derivatives are mainly bound to the lipoprotein fractions, with varying preferences for low-density lipoproteins (LDL) or high-density lipoproteins (HDL), and only the most polar derivatives showed significant accumulation in the high-density protein (HDP) fraction.

MATERIALS AND METHODS

Materials. Chemicals were analytical grade or better. Unless otherwise noted, chemicals were obtained from Sigma-Aldrich (Taufkirchen, Germany), Roth (Karlsruhe, Germany) or Merck (Darmstadt, Germany). Diethyl ether was dried and peroxides removed by Alumina B–Super I columns (ICN Biomedicals, Eschwege, Germany). Doubly demineralized water was used for all aqueous solutions. Blood products were obtained from the Bavarian Red Cross (Munich, Germany) and stored at 4°C for up to 4 weeks. A separation of occasionally existent chylomicrons was not necessary with either fractionation method used.

*Corresponding author email: hugo.scheer @lmu.de (Hugo Scheer)

Pigments. General: All preparations were carried out under green light (< 1 μE m^{-2} s^{-1}) and argon. Solvents were gassed with argon prior to and during use. Reactions were followed by absorption spectroscopy. Sodium ascorbate (~10 mg) was added as an antioxidant with all zinc insertion reactions. Zinc and palladium complexes were purified under argon on silica gel plates containing 1.5% sodium ascorbate. Pigments were stored dry in the dark and under argon at −20°C. Tetrapyrrole amounts are given in OD·mL units, namely, the product of the optical density (OD at the Q_y absorption maximum, 1 cm path length) and the volume (mL) of the pigment solution unless otherwise noted in diethyl ether ($OD{\cdot}mL_{DE}$). The C-13^2 epimers were not separated.

Esterified Mg-complexes: Chl and BChl were extracted with methanol from spray-dried *Spirulina platensis* (Behr Import, Bonn, Germany) and freeze-dried *Rhodospirillum rubrum* G9 (DSM No. 486; DSMZ, Braunschweig, Germany), respectively. 3-Acetyl-3-devinyl-chlorophyll ([3Ac]-Chl) was synthesized from BChl by oxidation with 2,3-dichloro-5,6-dicyano-*p*-benzoquinone (38). 3-Vinyl-3-deacetyl-bacteriochlorophyll ([3Vi]-BChl) was synthesized from BChl *via* 3-(1-hydroxy) ethyl-3-deacetyl-bacteriochlorophyll ([3HE]-BChl) according to Struck *et al*. (39). The pigments were purified by DEAE-Sepharose CL-6B (Amersham-Pharmacia, Freiburg, Germany) chromatography (40).

Nonesterified Mg-complexes: Chlorophyllide (Chlid) and bacteriochlorophyllide (BChlid) were obtained from Chl and BChl, respectively, by enzymatic hydrolysis of the phytyl ester moiety (41). The vector-bearing chlorophyllase (*Arabidopsis thaliana* ecotype Columbia) was provided by C. E. Benedetti (Brazilian Synchrotron Light Laboratory, Campinas, Brazil), and overexpressed in *Escherichia coli* (strain ER 2508) by U. Oster (University of Munich, Germany).

Metal-free derivatives: Pheophytin (Phe) and bacteriopheophytin (BPhe) were obtained by demetalation of Chl and BChl, respectively, with acetic acid (15 min, ambient temperature). The free acids, pheophorbide (Pheid) and bacteriopheophorbide (BPheid) were obtained by treating Chl and BChl, respectively, with trifluoroacetic acid (15 min, ambient temperature). As shown by absorption spectroscopy and HPTLC, the hydrolysates are free of colored by-products and did not require any additional purification.

Transmetalated chlorin derivatives: Zn-pheophytin (Zn-Phe) and Pd-pheophytin (Pd-Phe) were synthesized from Phe by the acetate method in acetic acid or methanol (42). Zn-pheophorbide (Zn-Pheid) was synthesized from Pheid by reaction with $Zn(OAc)_2$ and $Cd(OAc)_2$ (43). Pd-pheophorbide (Pd-Pheid) was obtained from Pheid by reaction with $Pd(OAc)_2$ in acetic acid (44).

Transmetalated bacteriochlorin derivatives: Zn-bacteriopheophytin (Zn-BPhe) and Zn-bacteriopheophorbide (Zn-BPheid) were synthesized from BPhe and BPheid, respectively, by reaction with $Zn(OAc)_2$ in acetic acid (42). Pd-bacteriopheophytin (Pd-BPhe) was obtained by transmetalation of Cd-BPhe (obtained from BPhe by the acetate method) with $PdCl_2$ in acetone (45). Pd-Bacteriopheophorbide (Pd-BPheid; WST09; Tookad®) was a gift of Negma-Lerads (Magny-Les-Hameaux, France). Tookad® as provided is designated WST09 in this investigation, while the chromatographically purified preparation (silica-60 column, gradient of 1–10% methanol in chloroform) is referred to as Pd-BPheid.

Others: Palladium 3^1-oxo-15-methoxycarbonylmethyl-rhodobacteriochlorin 13^1-(2-sulfoethyl) amide dipotassium salt (WST11; Stakel®, Steba Biotech, Toussus-Le-Noble, France) and 3^1-oxo-15-methoxycarbonylmethyl-rhodobacteriochlorin 13^1-(2-sulfoethyl)amide dipotassium salt ([H_2]-WST11) (35) were provided by A. Scherz (Weizmann Institute of Science, Rehovot, Israel). Pd-[3-(1-Hydroxy)ethyl]-bacteriopheophorbide ([3HE]-Pd-BPheid) was synthesized by reduction of Pd-BPheid with sodium borohydride in methanol according to the method for [3HE]-BChl (39). MS: 717.19 ($[M+H]^+$, $^{12}C_{35}H_{39}O_6N_4{}^{106}Pd$), 739.17 ($[M+Na]^+$, $^{12}C_{35}H_{38}O_6N_4Na^{106}Pd$) 761.16 ($[M\text{-}H+Na_2]^+$, $^{12}C_{35}H_{37}O_6N_4Na_2{}^{106}Pd$) *m/z*. UV–VIS in diethyl ether (DE) ($\epsilon_{rel.}$): 326 (0.555), 377 (0.508), 514 (0.127), 659 (0.130), 714 (1.000) nm. HpD (Photosan®) was from Seelab (Seehof Laboratorium, Wesselburenerkoog, Germany).

Spectroscopy. Absorption spectra were recorded with a UV 2401 PC Spectrometer equipped with an ISR 240-A Integrating Sphere Assembly (Shimadzu, Duisburg, Germany). Spectra were processed using Hyper UV 1.5 (Shimadzu) based on Spectacle (LabControl, Cologne, Germany). *In situ* absorption spectra of iodixanol gradients were recorded with a diode array detection (DAD) system consisting of a Tidas UVNIR/16-1024/100-1 diode array detector (J&M, Aalen, Germany) and a CLH 20 W lamp (J&M). The applied software was Spectralys 1.82 (J&M) based on Spectacle (LabControl). For pigment quantifications, identical absorption coefficients were assumed in the different BP fractions. Mass spectra were recorded with an LTQ Orbitrap Mass spectrometer (Thermo Electron, Dreieich, Germany). All samples were diluted 9:1 (vol/vol) with 1% (vol/vol) formic acid in methanol.

Blood (buffy coat) fractionation. Buffy coat fractionation by Ficoll®-Paque PLUS (GE Healthcare, Munich, Germany) was performed according to the manufacturer's instructions.

BP fractionations. (A) Lipoprotein fractionation by sequential density gradient ultracentrifugation (SDGU): The first method used to separate human BP was SDGU (46,47). Densities were determined by aerometry. When sample volumes were insufficient to completely fill two centrifuge tubes, adequate amounts of Tris-EDTA (TE)) buffer of identical density were added. All centrifugation steps were carried out at 10°C in No. 342414 Quick-Seal™ centrifuge tubes (39.0 mL; 1.0 × 3.5 in; Beckman, Palo Alto) and a Type 70 Ti fixed-angle rotor (8 × 39.0 mL; Beckman). For sealing and slicing of the tubes, Tube Sealer and Tube Slicer, respectively, were used (Beckman). The following TE buffers with different densities were used: TE buffer I (ρ = 1.0 g mL^{-1}): Tris-HCl (10 mM, pH 7.5) containing EDTA (1 mM); TE buffer II (ρ = 1.019 g mL^{-1}): 27.81 g NaCl plus 1 L of TE buffer I; TE buffer III (ρ = 1.063 g mL^{-1}): 96.25 g NaCl plus 1 L of TE buffer I; TE buffer H (ρ = 1.125 g mL^{-1}; 94.24 g KBr plus 1 L of TE buffer III); TE buffer IV (ρ = 1.21 g mL^{-1}): 234.93 g KBr plus 1 L of TE buffer III.

Tetrapyrroles (~250 $OD{\cdot}mL_{DE}$) were dissolved in 110 μL of a mixture of Cremophor EL (CrEL) and ethanol (1:1 vol/vol), which was diluted to 1.1 mL with normal saline immediately before addition to 55.0 mL BP (modified from Ref. [48]). Exceptions to this procedure were WST11 and HpD (~250 $OD{\cdot}mL_{methanol}$) which were dissolved in 50 mM phosphate buffer (PB; pH 7.2). All tetrapyrrole-loaded plasma samples were incubated under slow rotation for 3 h at ambient temperature.

After adjusting the density to 1.019 g mL^{-1} with TE buffer I, the BP was centrifuged at 120 000 ***g*** for 20 h. The top 15 mL was removed as the very low-density lipoprotein (VLDL) fraction. The subnatant density was adjusted to 1.063 g mL^{-1} with solid NaCl and centrifuged at 120 000 ***g*** for 24 h. The top 15 mL was removed as the LDL fraction. The subnatant density was adjusted to 1.21 g mL^{-1} with solid KBr and centrifuged at 120 000 ***g*** for 48 h. The top 15 mL was removed as the HDL fraction; the subnatant (ρ > 1.21 g mL^{-1}) contained the HDP fraction. The amounts of NaCl or KBr to increase the density of a solution from ρ^{old} to ρ^{new} were calculated according to the formula given in the supplement. For storage, the LDL and HDL fractions were dialyzed overnight at 4°C against several liters of TE buffer III (Servapor® tubing, MWCO: 12 000–14 000; Ø: 16 mm; Serva, Heidelberg, Germany). Samples were filtered sterile with Puradisc™ FP30 CA-S syringe filters (pore size: 0.45 μm; Whatman, Dassel, Germany).

HDL subfractionation into HDL_2 and HDL_3: HDL fractions were subfractionated into HDL_2 and HDL_3 fractions by dialyzing them overnight at 4°C against TE buffer H (Servapor® tubing, MWCO 12,000–14,000; Ø: 16 mm; Serva). The samples were centrifuged in sealed No. 342412 Quick-Seal™ centrifuge tubes (5.1 mL; 0.5 × 2.0 in; Beckman) in a VTi 80 vertical-tube rotor (Beckman) at ~260 000 ***g*** for 4 h. The top 0.75 mL was removed as the HDL_2 fraction; the lower 4.5 mL contained the HDL_3.

(B) Lipoprotein fractionation by iodixanol gradient ultracentrifugation (IGU): The alternatively used IGU fractionation of BP is based on the method of Graham (47) and Graham *et al*. (49). Most of the tetrapyrroles investigated (2.0 $OD{\cdot}mL_{DE}$) were dissolved in 40 μL of a mixture of CrEL and ethanol (1:1 vol/vol), which was diluted to 400 μL with normal saline (48) immediately before addition to 3.6 mL BP. Exceptions were WST11, [H_2]-WST11 and HpD (2.0 $OD{\cdot}mL_{methanol}$) which were dissolved in 50 mM PB (pH 7.2). [3HE]-WST09 was dissolved in CrEL/ethanol/normal saline (CES), DMSO or PB for comparative measurements. All tetrapyrrole-loaded plasma samples were incubated for 3 h under slow rotation at ambient temperature.

After incubation, each sample was mixed with 0.8 mL OptiPrep® (60% iodixanol solution; Sigma-Aldrich). No. 344075 Quick-Seal® Ultra-Clear® centrifuge tubes (5.1 mL; 0.5 × 2.0 in; Beckman) were

filled with 0.5 mL TE buffer I (see SDGU). Four milliliters of the sample was carefully layered under this solution, and finally 0.6 mL of pure OptiPrep® was layered at the bottom. The rest of the sample (0.8 mL) was kept at 4°C for further measurements. The sealed tubes were centrifuged in a VTi 80 vertical-tube rotor (8 × 5.1 mL; Beckman) at 260 000 ***g*** for 4 h. After centrifugation, several bands were clearly visible in the self-generated iodixanol gradients (Fig. S1).

The gradients were scanned *in situ* from top to bottom with a homemade DAD scanner, which allowed the recording of absorption spectra between 300 and 900 nm with a spatial resolution of ~0.33 mm (see Figs. S1–S3). The tubes were inserted vertically in a hole (Ø 14 mm) in a gray plastic block (*L* 30, *W* 30, *H* 92 mm). The top of the tube was positioned just below two opposite horizontal holes into which two optical fibers from the lamp and the DAD detector were fit. Using the tube as a cuvette with 12 mm path length, it was raised at a speed of ~20 mm min^{-1}, and a full spectrum was recorded every second. For calculation of pigment concentrations in BP fractions, the average Q_y absorption maximum of the pigment (arithmetic mean of the values for LDL and HDL) in each 3D densitogram was determined. A 2D densitogram was extracted at this wavelength out of the 3D data file, as well as a baseline at a position 100 nm to the red of this maximum. The difference 3D densitogram was resolved into Gaussians by a computer-generated fit (Origin 7.0; OriginLab, Northampton). Each curve was assigned to the different BP fractions, and the pigment distribution among the fractions was calculated by correlating the curves' areas.

Fractionation of gradient samples: The density of the collected samples was determined by measurement of the refractive index with an Abbé refractometer (Atago, Tokyo, Japan). The refractive indices (RI) were converted into densities by the following formula, generated from the best-fit line ($R = 0.99983$) of 11 comparison measurements with different mixtures of OptiPrep® and BP:ρ[mg/mL] = (RI – 1.06463)/0.27446.

Gel filtration. Tetrapyrrole binding analyses were performed by gel filtration with a Sephadex® G-25 Medium (GE Healthcare) column in a Pasteur pipette. The outlet of the column was connected to a flow-through cuvette (No. 178.010; Hellma, Müllheim, Germany). To achieve a constant flow in every run exactly 5.0 mL TE buffer III (see SDGU) was used as the mobile phase. Absorption spectra were recorded with the standard DAD system.

Lipoprotein analyses. Protein concentrations were determined with the Fluka® Advanced Protein Assay Reagent (Sigma-Aldrich). Phospholipid concentrations were determined with the Roche® Phospholipids Enzymatic colorimetric test (No. 691844; Roche, Mannheim, Germany). Cholesterol (ester) concentrations were determined with the Roche® Cholesterol Enzymatic colorimetric test (No. 2016630; Roche). Triglyceride concentrations were determined with the Roche® Triglycerides Enzymatic colorimetric test (No. 2016648; Roche). All analyses were performed in triplicate.

Transfer between lipoprotein fractions. Lipoprotein suspensions with the same density as BP ($\rho \approx 1.028$ g mL^{-1}) were generated by mixing of the following solutions obtained by SDGU (see above): 700 µL VLDL fraction, 700 µL dialyzed LDL fraction, 700 µL dialyzed HDL fraction, 1525 µL TE buffer I. In each experiment, only one of the lipoprotein fractions (LDL or HDL) was loaded with exogenous tetrapyrroles. The mixtures (3625 µL) were incubated for 3 or 24 h at ambient temperature, and analyzed by IGU (see above) after addition of 725 µL OptiPrep® solution.

RESULTS AND DISCUSSION

Pigments

The present study was aimed at investigating the influence of structural factors of Chl and BChl derivatives on their distribution among blood components. The following structural elements were varied (see Fig. 1 for structures and abbreviations): the central metal that governs excited state dynamics and ligand coordination (45,50,51), the presence or absence of the phytyl residue at C-17[3] that profoundly affects the polarity, the oxidation state of the macrocycle that influences the position of the Q_y absorption band in the red (chlorins) and NIR (bacteriochlorins) spectral region (52), the substituent at C-3 that has a modulating effect, *e.g.* on the redox potential (53) and optical properties (39), and the substituent at C-13 which in most cases forms the isocyclic ring E, but is open in the very polar taurinated WST11 pigments (35). HpD, the oldest licensed PDT photosensitizer (16), has been included for comparison.

Pigment distribution among blood fractions

In a first test, thrombocyte-enriched human blood (buffy coats) was incubated with WST09. Approximately three-quarters of the pigment were found after centrifugation in the topmost layer, a plasma–phosphate buffer saline–mixture (Fig. 2). The gradient fractions comprising cellular components contained only about one-tenth of the pigment, the remainder was located in the Ficoll layer, most probably because the pigment molecules were swept along by the large number of polymorphonuclear neutrophils (PMNs) and erythrocytes which crossed the Ficoll layer. In view of the small amounts of pigment in the cellular fraction, all subsequent experiments were focused on the pigment distribution among BP components, that is, the lipoprotein fractions and the HDP fraction that contains the serum albumin (HSA).

Pigment distribution among BP fractions: nonpolar tetrapyrroles

Human BP was incubated with the different pigments and subsequently fractionated by density gradient ultracentrifugation. The standard preparative fractionation method, namely SDGU (46,47), requires long periods (5 days) and is very demanding of material (55 mL BP, ~4 µmol pigment) and is thus unsuitable for a pigment distribution survey. It was, therefore, replaced in most cases by IGU (47,49). This method is much faster (1 day) and requires only very small quantities of materials (4 mL BP; ~30 nmol pigment). The IGU method is still considerably slower than electrophoretic methods (see Ref. [54]), but it avoids high dilution and is suitable for micropreparative purposes, even though the fractionation is somewhat less complete than with SDGU. For the current analytical study, however, this was compensated by the ability to analyze iodixanol gradients *in situ* with high spatial and spectral resolution (see Figs. S1–S3), which is facilitated by the high stability of these gradients (55): even after 18 h, there were no significant changes detectable in the band patterns. A further advantage is that the IGU method retains the osmolarity of the BP, whereas increasingly hyperosmotic salt concentrations are used in the SDGU method (47). The latter cause dehydration of the lipoproteins, as indicated by significantly increased densities of the SDGU fractions (LDL: 1.019–1.063 g mL^{-1}; HDL: 1.063–1.21 g mL^{-1}) relative to the respective IGU fractions in their native hydrated state in iodixanol gradients (LDL: 1.008–1.026 g mL^{-1}; HDL: 1.026–1.12 g mL^{-1}, see Fig. S2). The latter values, determined by refractive index measurements, are nearly identical with those given in the original publication of the IGU method (LDL: 1.010–1.030 g mL^{-1}; HDL: 1.030–1.14 g mL^{-1}) (49).

The separation was monitored by optical spectroscopy. Very reproducible 3D densitograms were obtained by scanning of the cylindrical part of the iodixanol gradients (central

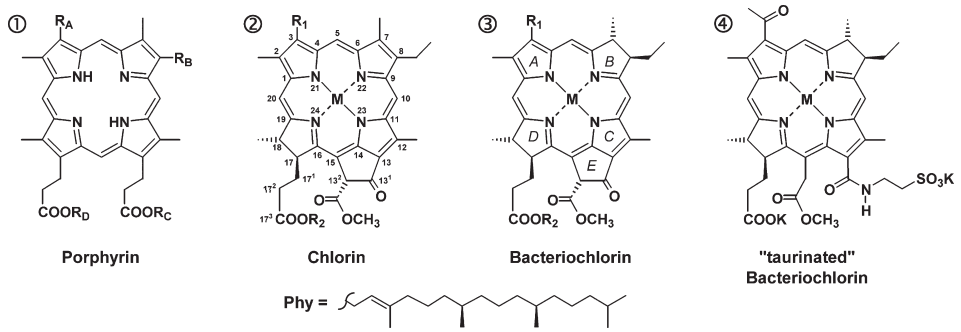

Pigment abbreviation	Formula	M	R_1	R_2	λ_{max} [nm]
HpD [a]	1	-	-	-	626*
Chl	2	Mg	vinyl	Phy	659
[3Ac]-Chl	2	Mg	acetyl	Phy	675
Zn-Phe	2	Zn	vinyl	Phy	653
Pd-Phe	2	Pd	vinyl	Phy	634
Phe	2	2 H	vinyl	Phy	667
Chlid	2	Mg	vinyl	H	660
Zn-Pheid	2	Zn	vinyl	H	652
Pd-Pheid	2	Pd	vinyl	H	635
Pheid	2	2 H	vinyl	H	667
BChl	3	Mg	acetyl	Phy	769
[3Vi]-BChl	3	Mg	vinyl	Phy	744
Zn-BPhe	3	Zn	acetyl	Phy	763
Pd-BPhe	3	Pd	acetyl	Phy	755
BPhe	3	2 H	acetyl	Phy	749
BChlid	3	Mg	acetyl	H	770
Zn-BPheid	3	Zn	acetyl	H	763
Pd-BPheid (WST09)	3	Pd	acetyl	H	755 (754)
[3HE]-Pd-BPheid	3	Pd	1-hydroxyethyl	H	714
BPheid	3	2 H	acetyl	H	749
WST11	4	Pd	-	-	747*
[H_2]-WST11	4	2 H	-	-	749*

Figure 1. Molecular structures and abbreviations of pigments. Numbering is according to IUPAC-IUB (96). The recommended but cumbersome omission-resubstitution nomenclature is replaced by placing the modified group in square brackets; thus, for example 3-devinyl-3-acetyl-Chl becomes [3Ac]-Chl. λ_{max} refers to the Q_y absorption maximum in diethyl ether (* in methanol); further spectral information of all pigments is given in Table S1. Pigments with an isocyclic ring (formulas 2 and 3) are generally present as 13^2-epimer mixtures; but only the 13^2*R*-epimers are shown, which are usually present in large excess over the 13^2*S*-epimers. [a]HpD is a mixture of di- and oligomeric compounds (17); only the basic porphyrin structure is shown.

40 mm). In the two hemispherical areas at the top and bottom of the tubes, quantification was less reliable and only qualitative absorption spectra were obtained, due to the increased scattering of the walls and the shortening of the optical pathway. The pigment concentrations in VLDL fractions, which were located completely in the upper hemisphere could, therefore, not be measured satisfactorily *in situ*. The estimation of the pigment concentrations in the HDP fractions was further complicated by the presence of an overwhelming amount of heme in these fractions.

The results obtained by IGU for all pigments with an intact isocyclic ring E are shown in Fig. 3. In average BP, the combined pigment content in the VLDL and HDP fractions of each of these pigments was ≤10% as determined by the SDGU method; therefore, results are only given for the LDL and HDL fractions. In extremely high-fat BP charges, the pigment content in the VLDL fraction amounted to >40%. However, the relative pigment distribution among the respective LDL, HDL and HDP fractions remained unaltered. The preferential accumulation in LDL and HDL emphasizes their relevance as transport vehicles for lipophilic to moderately hydrophilic photosensitizers (like WST09) in the vascular

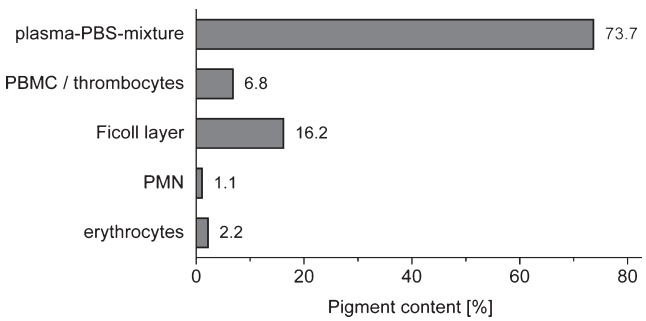

Figure 2. Distribution of WST09 among human blood fractions. Buffy coats were fractionated by underlayering with Ficoll®-Paque Plus and subsequent centrifugation. PBMC = peripheral blood mononuclear cells.

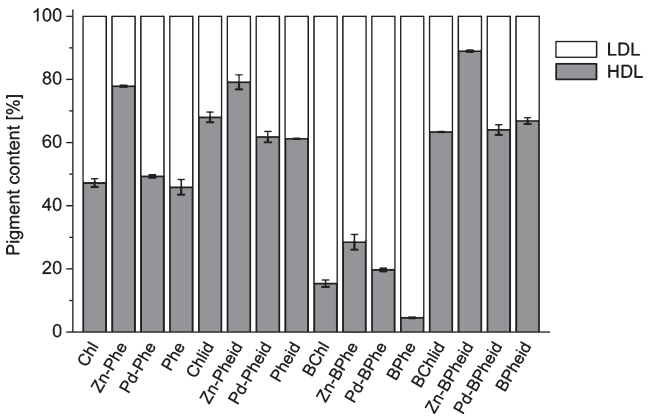

Figure 3. Pigment distribution of selected tetrapyrroles between LDL and HDL fractions. BP was incubated with selected pigments and fractionated by IGU. The pigment contents of the respective LDL and HDL bands in the formed iodixanol gradients were analyzed spectroscopically by *in situ* scanning (see Materials and Methods, BP fractionations and Supporting Information for details). Means ± SEM, n = 2–3.

system. Similar results have been reported for a series of porphyrinic PDT sensitizers with up to 8 carboxyl groups (56–58).

The distribution of pigments between LDL and HDL fractions of human BP shows some clear patterns. The phytyl residue resulted in a preferential pigment accumulation in the LDL fraction; this effect was much more pronounced in BChl compared with Chl derivatives. The two extremes were the Zn-Phe/Zn-Pheid pair that showed only a minor difference and the BPhe/BPheid pair where the LDL/HDL ratios were nearly reversed (21:1 for BPhe *vs* 1:2 for BPheid). By contrast, no significant difference was detectable between the Chlid and BChlid derivatives that have a free propionic acid residue at C-17. There was also a distinct effect of the central metal: the Zn-derivatives accumulated more in the HDL fraction than their respective Mg-, Pd- and H_2-analogs. The latter three pigments exhibited in most cases a similar pigment distribution between HDL and LDL, with the notable exception of BPhe, which was almost completely located in the LDL fraction (see above). The *in situ* scanning showed that there was no pigment aggregation in any of these fractions, as judged by the absence of redshifted absorption bands (see Fig. S3).

The pigments esterified with phytol are probably anchored by this long hydrocarbon chain to the lipoprotein surface. This might be facilitated by the less charged membrane surface and/or the higher cholesterol content of the LDL compared to the HDL membrane, thereby rationalizing the higher accumulation of these esterified pigments in LDL. Due to steric or electronic effects, the BChl derivatives may be anchored more deeply into the membrane than the respective Chl derivatives (the C-3 residue contributes only little to pigment binding, see Influence of structural details: Chl vs BChl).

At the near-neutral pH of the experiments, the nonesterified pigments carry a negatively charged carboxylate group at C-17^3, which probably imposes a different orientation of the pigment in which the now less polar macrocycle (relative to the C-17 substituent) penetrates into the membrane, and the carboxylate interacts with the positively charged choline head groups of the phosphatidylcholins and sphingomyelins. Such a model is supported by the location of bacteriochlorin *a*, which possesses three negative charges at rings C and D, near the membrane surface of liposomes (59). It also explains the similar pigment distribution pattern of all tested tetrapyrroles without a phytyl residue, that are all Chlid and BChlid derivatives (with the exception of the Zn-complexes, see Specific interaction of Zn-complexes with HDL).

Specific interaction of Zn-complexes with HDL

The (relative) enrichment of Zn-complexes in the HDL fraction (see Pigment distribution among BP fractions: nonpolar tetrapyrroles), compared to other metal complexes and the free bases, was accompanied by a redshift of the Q_y absorption maximum, relative to its position in LDL (see Fig. S4). This effect was least pronounced with Zn-BPhe, which was also the Zn-complex that showed the lowest accumulation in the HDL fraction. In the Pd-derivatives, the respective spectral shifts were very weak, and of variable direction, and the shifts were negligible for the metal-free derivatives. Intermediate redshifts were observed for the Mg-derivatives, the least pronounced again with the "bacteriopheophytin derivative," BChl. By analogy with the respective Zn-complex, the latter showed the lowest enrichment in the HDL fraction among all Mg-complexes. The extent of all observed redshifts, therefore, seems to be directly related to the pigment distribution. This preferential binding prompted us to further subfractionate the HDL, using again Zn- and Pd-BPheid as test pigments. HDL_2 and HDL_3 subfractions were obtained by SDGU. The ratio of the pigment contents in HDL_3 *vs* HDL_2 was 1.13 ± 0.01 (normalized to the same total HDL_2 and HDL_3 lipoprotein mass), irrespective of the applied pigment. The specific binding of Zn-BPheid must therefore occur in both subfractions at comparable levels. The bound pigment content in these two HDL subfractions seems to be directly correlated with the total lipoprotein surface: The surface-to-mass ratio of an average HDL_3 particle (∅: 8 nm; m: 200 kDa [60]) is 1.15 times higher than that of an average HDL_2 particle (∅: 10 nm; m: 360 kDa [60]).

Further support for a specific binding of Zn-complexes to HDL comes also from a comparison of the pigment–lipoprotein ratios of Zn- and Pd-BPheid. Molar lipoprotein concentrations in HDL and LDL were estimated by summing up the protein, phospholipid, total cholesterol and triglyceride determinations, while molar pigment concentrations were measured by their absorptions using an integrating sphere. The precision of the method is limited by the need to estimate the average lipoprotein particle mass, and by the assumption of the same extinction coefficients of the pigments in the lipoproteins as in CES (Table 1). According to this analysis, HDL binds approximately three times more Zn-BPheid than Pd-BPheid. By contrast, the number of tetrapyrrole molecules bound to individual LDL particles was almost identical for Zn- and Pd-BPheid. The coordination ability of the central metal therefore only influences HDL binding, while LDL can serve as a control.

This differential behavior of pigments with Zn^{2+} and Mg^{2+} as central metal parallels observations of Szczygiel *et al.* (61) on the tissue distribution of Chlid and its Zn-derivative, Zn-Pheid, where the Zn-complex showed slower uptake and loss from mice after interperitoneal injection. While aggrega-

Table 1. Molar ratios of bound pigment per lipoprotein particle. Pd- or Zn-BPheid were added to BP before SDGU fractionation. Extinction coefficients were determined in CES relative to the known ones in DE (45). The average lipoprotein particle masses used for LDL and HDL were 2500 and 250 kDa, respectively (60).

Pigment	ϵ (M^{-1} cm^{-1}) in DE	ϵ (M^{-1} cm^{-1}) in CES	Pigment per lipoprotein particle (mol mol^{-1}) LDL	HDL
Pd-BPheid	92 000	56 000	3.57 ± 0.07	0.65 ± 0.01
Zn-BPheid	67 700	46 000	3.43 ± 0.07	1.84 ± 0.02

Pd-BPheid = Pd-bacteriopheophorbide; Zn-BPheid = Zn-bacteriopheophorbide; BP = blood plasma; SDGU = sequential density gradient ultracentrifugation; CES = CrEL/ethanol/normal saline; DE = diethylether; LDL = low-density lipoprotein; HDL = high-density lipoprotein.

tion, active excretion and degradation are involved in the whole animal, these processes can be excluded in the BP fractions. This, therefore, points to a distinct binding difference among the two central metals.

Coordination of central metal

In the bacteriochlorins, additional information on the binding situation can be obtained by an analysis of the Q_x absorption which is very sensitive to the electron densities of their central metals, and thereby to their coordination state (62). Studies in solution (45,63,64), with synthetic (65) and natural proteins (66) indicate characteristic regions for four-, five- and six-fold coordinated central metals that, in spite of additional influences (*e.g.* solvent polarity), do not overlap. According to this classification, the Mg- and Zn-derivatives had five-fold coordinated central metals in all lipoproteins (Fig. 4). The exact position within the range defining five-fold coordination allows furthermore a rough estimate of the average polarity prevailing in the pigment environment. The position of the Q_x absorption band was nearly identical in HDL and LDL fractions for both Mg-complexes while, for both Zn-complexes, it was significantly redshifted in HDL fractions compared to LDL fractions, thus indicating a less polar environment in the latter. The coordination state also influenced the stability of pigment binding as investigated by gel filtration experiments. LDL samples lost more pigment (3–6%) than HDL samples (1.5–2.5%), and the pigment loss was always less for Zn-BPheid than for Pd-BPheid. The Q_x absorption band of the Pd-derivatives was buried under the red-most carotenoid band and its position could not be accurately determined; however, Pd usually does not bind any extra ligands (67), which in tetrapyrroles resembles the binding situation of the free bases.

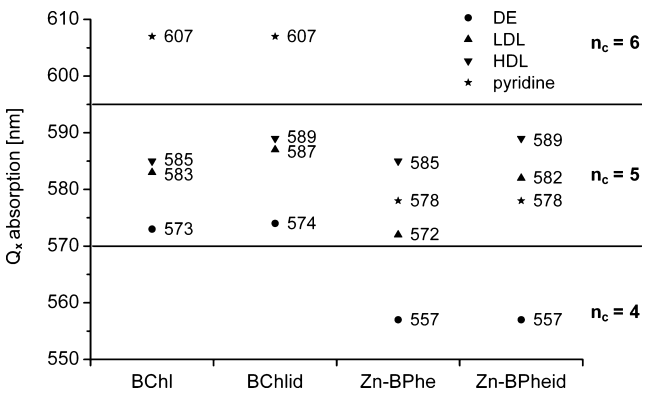

Figure 4. Positions of the Q_x absorption maxima of Mg- and Zn-bacteriochlorins in HDL and LDL fractions. Values in diethyl ether and pyridine are given for comparison. The horizontal lines indicate the ranges for the different coordination states of the central metal (n_c = 4, 5 or 6), corresponding to 0, 1 or 2 extra ligands.

The differential effects of Zn- compared to Mg-complexes may relate to the fact that Mg binds extra ligands very strongly (68); it may therefore carry a water molecule irrespective of the environment. There are, by contrast, "naked" Zn-tetrapyrroles in which the central metal lacks extra ligands; they are, therefore, more responsive to environment changes. A specific binding of the Zn-complexes may also explain the observation that the Mg-derivatives showed nearly identical distributions as the respective Pd- and H_2-derivatives, in spite of their different coordination state. This is reminiscent of the binding of (bacterio)chlorophylls in photosynthetic pigment proteins, where binding is rescued in mutants where enough space is provided, in a hydrophobic pocket, to bring along a small ligand (52). This difference between the Zn- and Mg-derivatives is further support of a special binding situation in the HDL fraction that favors Zn over Mg as the central metal, which may be related to their difference in hardness (69). Apolipoproteins might be binding partners that control this selectivity for HDL. Further support for such a special binding was the occurrence of a Krasnovskii reaction, a photoreduction requiring an amino group in the immediate vicinity of the tetrapyrrole (70). This study will be published separately together with the photochemistry of the sensitizers in the different BP fractions.

Influence of structural details: Chl *vs* BChl

There was a remarkable difference in the pigment distribution between LDL and HDL fractions for the Chl/BChl pair (see Fig. 3). These two pigments differ in two details of their chemical structure, *viz*. the oxidation state of the macrocycle and the substituent at C-3, which is a vinyl group in Chl and an acetyl group in BChl. Therefore [3Ac]-Chl and [3Vi]-BChl were tested as well, in which the substituents at C-3 are reversed. This reverses the polarities, too, if judged by their chromatographic mobilities, because the acetyl group is considerably more polar than the vinyl group (38), while the oxidation state has only little influence on the polarity (71).

Surprisingly, the pigment distribution was only slightly influenced by the side chain at C-3, but much more so by the oxidation state of the macrocycle (Fig. 5). Irrespective of the C-3 residue, the presence of a chlorin macrocycle more than tripled the pigment content of the HDL fraction relative to a bacteriochlorin macrocycle, while the presence of a 3-acetyl group led only to a slight increase in the pigment content in the HDL fraction relative to a 3-vinyl group. These findings support the above-mentioned assumption (see Pigment distribution among BP fractions: nonpolar tetrapyrroles) that the bacteriochlorin derivatives are more deeply anchored into the lipid membrane than the respective chlorin derivatives. The reason for this distinction is presently unclear. During

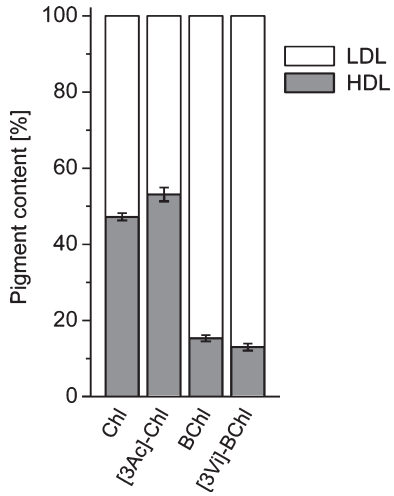

Figure 5. Pigment distribution of Chl, [3Ac]-Chl, BChl and [3Vi]-BChl between LDL and HDL fractions. BP was incubated with selected pigments and fractionated by IGU. The pigment contents of the respective LDL and HDL bands in the formed iodixanol gradients were analyzed spectroscopically by *in situ* scanning. Means ± SEM, $n = 2–3$.

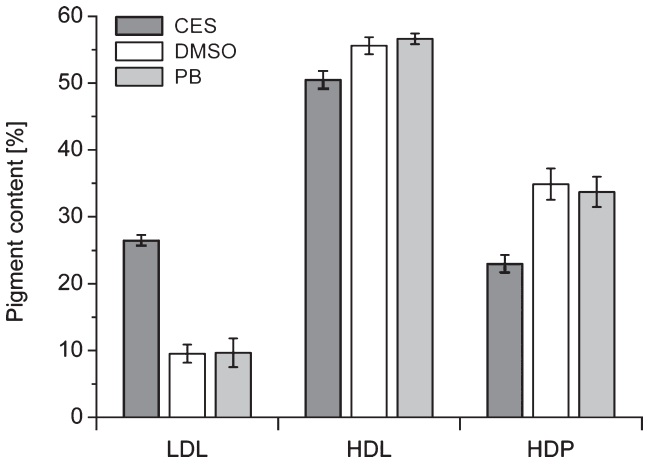

Figure 6. Influence of pigment insertion system (CES, DMSO and PB) on the distribution of [3HE]-Pd-BPheid among LDL, HDL and HDP fractions. BP was incubated with [3HE]-Pd-BPheid dissolved in either CES, DMSO or PB and fractionated by IGU. The pigment contents of the respective LDL, HDL and HDP bands in the formed iodixanol gradients were analyzed spectroscopically by *in situ* scanning. Means ± SEM, $n = 2–3$.

chromatography on reverse phase material, bacteriochlorins moved consistently slower than chlorins with otherwise identical structure, indicating a less polar structure of the former, which may relate to changes in the conjugated π-system (Fig. 1). However, steric factors and a differential flexibility at ring B may also contribute. This is another indication for a specific interaction of pigments with lipoproteins that relies on structural details rather than on gross changes in their lipophilicity. The interaction of pigments with the lipid surface of lipoproteins is often treated as a phase distribution between an aqueous and a lipid phase (72). Pigment lipophilicity correlates, however, only for structural homologs with their measured binding constants on membranes or liposomes; in other cases the correlation is poor (73).

Influence of the solubilizer

As all the aforementioned pigments are only poorly soluble in aqueous media, they have to be dissolved in organic solvents or detergents for intravenous injection. To analyze the effect of the application method on the pigment distribution, Pd-[3-(1-hydroxy)ethyl]-bacteriopheophorbide ([3HE]-Pd-BPheid) was synthesized that has intermediate solubility in aqueous media between WST09 and the very hydrophilic WST11. Judged from the position and shape of the Q_y absorption band (not shown), [3HE]-Pd-BPheid was monomeric in aqueous solutions at pH ~8, in contrast to its precursor WST09. When [3HE]-Pd-BPheid was applied in CES (a mixture of CrEL, ethanol and normal saline, see Materials and Methods), ~50% was found in the HDL fraction, and ~25% each in the LDL and HDP fractions (Fig. 6). If, however, [3HE]-Pd-BPheid was added in DMSO or PB, its content in the HDL and HDP fractions was increased to ~55% and ~35%, respectively, while only ~10% remained in the LDL fraction. The application system also affected the partitioning of WST09: when applied in DMSO, the pigment content in the LDL fraction was 10.5% lower than when it was added in CES, while the contents in all other fractions increased slightly (VLDL: +1.5%; HDL: +4.5%; HDP: +4.5%). Comparable results have also been reported for tin ethyl etiopurpurin (SnET2); it accumulated preferentially in the LDL fraction if added in CrEL relative to its application in ethanol, DMSO, cyclodextrins or liposomes (74–77). The pigment distribution among the two lipoprotein fractions, LDL and HDL, was almost identical for [3HE]-Pd-BPheid (HDL: ~66%) and Pd-BPheid (HDL: ~64%), indicating again the small impact of the C-3 substituent on the distribution patterns.

This preferential pigment accumulation in LDL has been attributed to a preferential fusion of CrEL with an LDL subfraction (78). Alternatively, a buoyant density shift in HDL particles is induced by CrEL, which would then mimic an LDL subfraction (79); this is supported by a slightly increased carotenoid content in the LDL fraction of BP incubated with CES (data not shown). Further support for a lipoprotein reorganization came from a small, but distinct density shift in the maximum absorption of the pigment in the LDL fraction by ~0.01 g mL^{-1} (corresponding to ~1 mm in the iodixanol gradient), relative to the maximum of the carotenoid absorption (Fig. 7); the effect was absent if the pigment was added in DMSO or PB. In the absorption spectra at these two positions, the intensity ratio of the BChl and the carotenoid main bands was changed accordingly. This effect was particularly apparent for all pigments, like BChl, that partition preferentially in the LDL fraction (see Fig. 3). It was detectable in all BP charges used in this study, possibly because individual LDL subfraction patterns, which can vary widely, tend to equilibrate within a short time (80). These data indicate that the (B)Chl derivatives and carotenoids partition differently among the subfractions in the presence of CrEL. The CrEL-based CES was used in this work as the standard application medium. It has been developed as an alternative to DMSO that is principally an excellent solvent but has multiple adverse effects (81,82), yet CrEL should not be seen as an inert solubilizer (83).

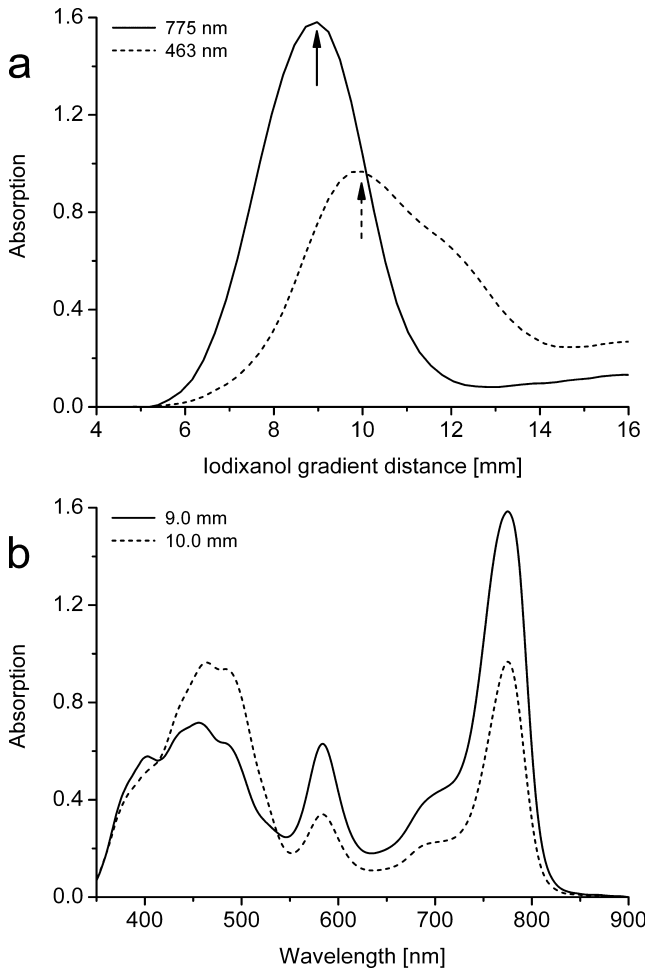

Figure 7. Spectroscopic indication for lipoprotein reorganization by Cremophor® EL. BP was incubated with BChl and fractionated by IGU. Densitograms (a) of the LDL band at the Q_y absorption maximum of BChl (775 nm) and at the carotenoid absorption maximum (463 nm) obtained by scanning of the tube along the axis, and absorption spectra (b) at the respective densitogram maxima (9.0 and 10.0 mm, respectively).

Influence of other parameters

A significantly higher concentration of WST09 in HDL has been reported for fetal calf serum (35) than was observed here for human plasma, indicating that the pigment distribution in blood serum is species dependent. Similar results have been reported for other sensitizers (84) which relate to a different chemical composition of the lipoproteins. It should be noted, however, that such comparisons require otherwise identical conditions. It has been shown, for example, that the pH (85) or concentrations of pigment and solvent applied are critical (86). These factors were kept constant throughout this study to obtain internal consistency. We furthermore verified, using WST09, that the partitioning among the plasma fractions was not affected within an eight-fold concentration range (quarter to double standard). These variations are relatively small, however, when compared with the more than 10-fold higher concentrations used by Brandis *et al.* (35). Aggregation at higher concentrations may contribute to rapid excretion of the pigment in PDT (A. Scherz, private communication, 2009) (87).

Distribution of polar bacteriochlorin derivatives among BP fractions

Recently, two extraordinarily hydrophilic bacteriochlorin derivatives have become accessible: the taurinated Pd-complex WST11 and its metal-free analog, [H_2]-WST11. Their distribution among BP fractions was compared to that of the much less polar WST09, and to the classical PDT photosensitizer HpD (in the form of Photosan®). Approximately 50% of HpD was found in the HDP fraction, and over 80% and 90% of WST11 and [H_2]-WST11, respectively, with serum albumin being the most likely carrier (Fig. 8). In contrast only ~15% of WST09 were located in this fraction (see above).

As in the case of [3HE]-Pd-BPheid (see Influence of the solubilizer), the pigment concentration of the three polar pigments in the HDP fraction was high enough for a reliable determination by IGU; three of the above-mentioned pigments (WST09, WST11, HpD) were, therefore, used to compare the IGU with the classical SDGU for BP fractionation. When using the SDGU method, reduced pigment content in the HDP fraction was consistently observed relative to the IGU method. This effect was most pronounced for WST11, where the pigment content in the HDP fraction was halved, in favor of the LDL and HDL fractions. This effect, which appears to increase with increasing hydrophilicity (water solubility) of the pigment, may be due to a less preferred pigment binding to lipoproteins. This is supported by the distribution pattern of [3HE]-Pd-BPheid, which is slightly more water soluble than WST09. If applied as a CES solution, the pigment content in HDP was ~9% higher than for WST09, but still ~18% less than for HpD if dissolved in PB. The correlation of increasing pigment polarities with increasing pigment concentrations in the respective HDP fraction has already been reported for other pigments (58,88). Preferential binding of lipophilic photosensitizers to plasma lipoproteins and of hydrophilic photosensitizers to serum albumin was shown for a series of sulfonated derivatives of tetraphenylporphine (89).

Interestingly, the ratios of all tested polar (see Fig. 8) and nonpolar (see Fig. S5) tetrapyrroles in the LDL and HDL

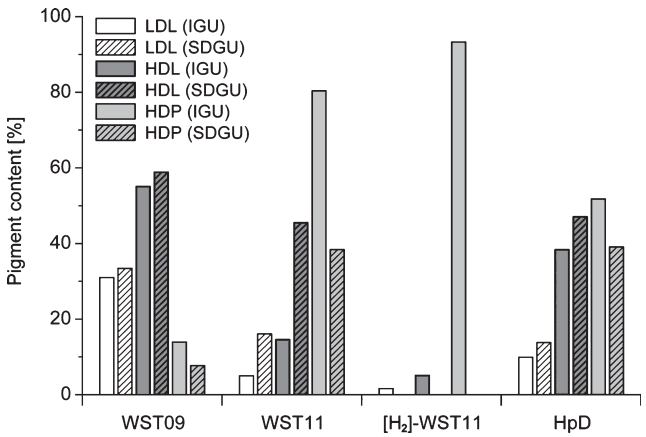

Figure 8. Influence of fractionation method on the distribution of WST09, WST11 and HpD among LDL, HDL and HDP fractions. BP was incubated with selected pigments and fractionated by IGU. The pigment contents of the respective LDL, HDL and HDP bands in the iodixanol gradients were analyzed spectroscopically by *in situ* scanning. [H_2]-WST11 was fractionated by IGU only. IGU = plain columns; SDGU = hatched columns.

fractions were identical within the error limits for both applied fractionation methods. Both methods separate BP components according to their buoyant densities, but while IGU conditions are isotonic with BP, those of SDGU are highly hypertonic. Similar fractionation methods utilizing high-salt solutions did not alter the pigment distribution among lipoproteins (90). This suggests that the pigment affinities of some HDP components (probably serum albumin) are reduced at the high salt concentrations used in SDGU, while those of the different lipoproteins are either unaltered or at least modified in a similar way compared to isotonic conditions.

Transfer between lipoprotein fractions

In our experience, the exchange of chlorophylls between vesicular or micellar compartments can be rather slow. It was of interest, therefore, to study the exchange kinetics of pigments among the BP fractions. The experiments were carried out with two pigments. One was Pd-BPheid, which is currently scrutinized for vascular targeted phototherapy with very short intervals between injection and irradiation, or between multiple irradiations, which may cause depletion in individual compartments (91,92). The other was Zn-BPheid, which partitioned differently among LDL and HDL fractions than the Mg-, Pd- and H_2-derivatives (see Pigment distribution among BP fractions: nonpolar tetrapyrroles and Specific interaction of Zn-complexes with HDL). Pigment-loaded LDL or HDL fractions were prepared by SDGU, and mixed with the complementary empty lipoprotein complement. The mixtures were incubated for 3 or 24 h at ambient temperature, and then separated by IGU and analyzed for their pigment contents.

Both of the tetrapyrroles tested were fully equilibrated between the respective LDL and HDL fractions within 24 h (Fig. 9). The partitioning was identical to that observed after incubation of the original BP with the respective pigment, and no significant difference could be measured whether the LDL or HDL fraction was pigment-loaded prior to incubation. Even after incubation for 3 h (plus ~15 min for sample preparation), the pigments provided originally in the HDL fractions were entirely equilibrated. The reverse pigment transfer from LDL to HDL was not fully completed at the end of this period; however, in the case of Pd- and Zn-BPheid ~94% and ~97%, respectively, of the transfer had already taken place. This gives for both pigments an upper limit for the kinetic constants for equilibration of less than 1 h. Fast exchange has also been reported for tin etiopurpurin (93) and zinc phthalocyanine (94). On the other hand, only moderately polar carotenoids like lutein exchange readily between human VLDL and HDL, while nonpolar ones like carotenes or lycopene gave no measurable interlipoprotein transfer (95).

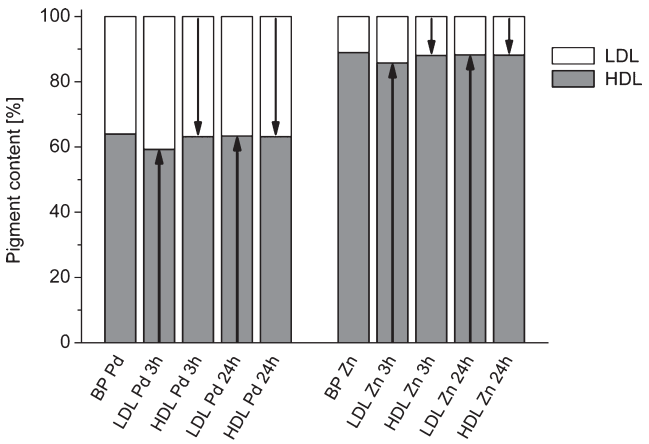

Figure 9. Redistribution of Pd- and Zn-BPheid between LDL and HDL fractions. BP: pigment distribution in the same BP batch, determined by standard IGU (see Fig. 3). LDL and HDL indicate the pigment-loaded BP fraction at the onset of the experiment (Pd: Pd-BPheid; Zn: Zn-BPheid). The fractions were incubated for either 3 or 24 h. Arrows indicate the increase or decrease in the respective pigment concentration, relative to the pigment concentrations at the onset of the experiment (see Materials and Methods, Transfer between lipoprotein fractions for details).

CONCLUSIONS

Iodixanol-gradient ultracentrifugation is, in combination with *in situ* scanning, a versatile and comparably rapid method for investigating the distribution of photosensitizers among the different BP fractions. Using standardized conditions and Cremophor® EL as solubilizing medium, the structural effects among the 21 (bacterio)chlorophyllous sensitizers can be summarized as follows: (1) Only the most polar derivatives that are readily soluble in water accumulate to a significant degree in the HDP fraction. (2) Decreasing polarity results in an increasing accumulation in the LDL relative to the HDL fraction. However, specific binding has been observed for Zn^{2+}-complexes, and when comparing Chl and BChl derivatives with identical substituents. (3) The latter difference is absent in derivatives with a free propionic acid at C-17, Chlids and BChlids. (4) The speed of the fractionation allowed for estimating an upper limit for the equilibration periods among HDL and LDL fractions in the range of 1 h. Specific binding will therefore probably not affect drug delivery and action on longer time scales. Faster analytical methods (54) can possibly reduce this time scale, which may be relevant, in particular in vascular targeted PDT using very short accumulation and irradiation times. (5) Aggregation of pigments has, to our surprise, never been observed in BP fractions at the concentrations used in this study. Concerns that the photophysics *in situ* may be influenced by aggregations therefore seem irrelevant. (6) Dark oxidation, which occurs readily in solution, seems to be impeded in lipoproteins.

The results should be helpful in two ways for the rational design of photosensitizers for accumulation in the different blood components. One aspect is that the highly polar WST11 is set apart from all other (B)Chl-derived pigments, including the moderately polar [3HE]-Pd-BPheid, as the only pigment that is not mainly carried by the lipoprotein fractions of human BP. The damage to these fractions, as part of the photodynamic action, or as an unwanted side-reaction, will, therefore, also be different. The second aspect is that although the two main lipoproteins, LDL and HDL, discriminate among most pigment derivatives tested only on the basis of their bulk polarity, the photosensitizer distribution can be

influenced by certain structural features, in particular the central metal. Both aspects should be considered in fine-tuning PDT, and warrant further studies to correlate the pigment distributions in human BP with intracellular localization and photosensitizing efficacy.

Acknowledgements—This work was supported by the Hans-Fischer-Gesellschaft e. V. München (Munich, Germany), by a PhD grant to J.D. We are indebted to A. Scherz (Weizmann Institute of Science, Rehovot) for providing WST11, and to R.J. Porra (CSIRO, Canberra) for help in preparing this manuscript. WST09 was provided by Steba N.V. through collaboration with Negma-Lerads.

SUPPORTING INFORMATION

Additional Supporting Information may be found in the online version of this article:

Figure S1. Home-made DAD scanner (schematic) for iodixanol gradients of tetrapyrrole-loaded human blood plasma.

Figure S2. Iodixanol gradient fractionation of blood plasma loaded with Pd-BPheid. Photograph (left) and schematic band pattern (center, colored according to the isolated fractions) after centrifugation (see Materials and Methods). The colors of the faint pink HDL fraction and the milky white VLDL fraction are not adequately reproduced by the digital camera. The density distribution along the vertical axis (right) before and after centrifugation, has been obtained from the refractive index. For refractive index measurements the tube content (5.1 mL) was portioned into 51 fractions of 100 μL. A linear calibration curve for conversion of refractive indices into densities was created separately.

Figure S3. Iodixanol gradient fractionation of blood plasma loaded with Pd-BPheid. Color-coded spectral profile (top) along the vertical axis of the tube shown in Fig. S2 (top of tube = 0 mm). Pigment distribution (bottom left) along the vertical axis obtained as the difference of the absorption profiles at 757 nm (Q_y absorption maximum of Pd-BPheid) and 857 nm (scattering), and its Gaussian deconvolution (bottom right). Ery = erythrocytes.

Figure S4. Wavelength shifts of the Q_y absorption maxima between LDL and HDL fractions. Positive values correspond to a redshift in the HDL *vs* the LDL fraction. λ-scatter (not shown) < 1 nm ($n = 2$–3).

Figure S5. Pigment distribution of BChl, Pd-BPheid (WST09) and Zn-BPheid between the LDL and HDL fractions depending on the fractionation method. Selected pigments are representative of strong, intermediate and weak accumulation in the LDL fraction. Means ± SEM; IGU (all pigments): $n = 2$, SDGU (BChl): $n = 2$, SDGU (Pd-BPheid): $n = 7$, SDGU (Zn-BPheid): $n = 4$.

Table S1. Spectral properties of used tetrapyrroles in diethyl ether (* in methanol). Maxima of main absorption bands (nm) and (in brackets) their absorptions normalized to the intensity of the (0-0) transition of the respective Q_y absorption band (for HpD to the intensity of the Soret band).

Please note: Wiley-Blackwell are not responsible for the content or functionality of any supporting materials supplied by the authors. Any queries (other than missing material) should be directed to the corresponding author for the article.

REFERENCES

1. Ackroyd, R., C. Kelty, N. Brown and M. Reed (2001) The history of photodetection and photodynamic therapy. *Photochem. Photobiol.* **74**, 656–669.
2. Moan, J. and Q. Peng (2003) An outline of the history of PDT. In *Comprehensive Series in Photochemistry and Photobiology, 2: Photodynamic Therapy* (Edited by T. Patrice), pp. 3–17. Royal Society of Chemistry, Cambridge, UK.
3. Kessel, D. (2004) Delivery of photosensitizing agents. *Adv. Drug Deliv. Rev.* **56**, 7–8.
4. Solban, N., I. Rizvi and T. Hasan (2006) Targeted photodynamic therapy. *Lasers Surg. Med.* **38**, 522–531.
5. Juzeniene, A., Q. Peng and J. Moan (2007) Milestones in the development of photodynamic therapy and fluorescence diagnosis. *Photochem. Photobiol. Sci.* **6**, 1234–1245.
6. Hamblin, M. R. and E. L. Newman (1994) On the mechanism of the tumour-localising effect in photodynamic therapy. *J. Photochem. Photobiol. B, Biol.* **23**, 3–8.
7. MacDonald, I. J. and T. J. Dougherty (2001) Basic principles of photodynamic therapy. *J. Porphyr. Phthalocyan.* **5**, 105–129.
8. Wilson, B. C. and M. S. Patterson (2008) The physics, biophysics and technology of photodynamic therapy. *Phys. Med. Biol.* **53**, R61–R109.
9. Rosenbach-Belkin, V., L. Chen, L. Fiedor, I. Tregub, F. Pavlotsky, V. Brumfeld, Y. Salomon and A. Scherz (1996) Serine conjugates of chlorophyll and bacteriochlorophyll: Photocytotoxicity in vitro and tissue distribution in mice bearing melanoma tumors. *Photochem. Photobiol.* **64**, 174–181.
10. Spikes, J. D. and J. C. Bommer (1991) Chlorophyll and related pigments as photosensitizers in biology and medicine. In *Chlorophylls* (Edited by H. Scheer), pp. 1181–1204. CRC Press, Boca Raton, FL.
11. Chen, Y., G. Li and R. K. Pandey (2004) Synthesis of bacteriochlorins and their potential utility in photodynamic therapy (PDT). *Curr. Org. Chem.* **8**, 1105–1134.
12. Brandis, A., Y. Salomon and A. Scherz (2006) Bacteriochlorophyll sensitizers in photodynamic therapy. In *Chlorophylls and Bacteriochlorophylls: Biochemistry, Biophysics, Functions and Applications* (Edited by B. Grimm, R. Porra, W. Rüdiger and H. Scheer), pp. 485–494. Springer, Dordrecht.
13. Brandis, A., Y. Salomon and A. Scherz (2006) Chlorophyll sensitizers in photodynamic therapy. In *Chlorophylls and Bacteriochlorophylls: Biochemistry, Biophysics, Functions and Applications* (Edited by B. Grimm, R. Porra, W. Rüdiger and H. Scheer), pp. 461–483. Springer, Dordrecht.
14. Moser, J. G. (1998) *Photodynamic Tumor Therapy: 2nd and 3rd Generation Photosensitizers*. OPA, Amsterdam.
15. Pandey, R. K., S. Constantine, T. Tsuchida, G. Zheng, C. J. Medforth, M. Aoudia, A. N. Kozyrev, M. A. J. Rodgers, H. Kato, K. M. Smith and T. J. Dougherty (1997) Synthesis, photophysical properties, *in vivo* photosensitizing efficacy, and human serum albumin binding properties of some novel bacteriochlorins. *J. Med. Chem.* **40**, 2770–2779.
16. Dougherty, T. J., C. J. Gomer, B. W. Henderson, G. Jori, M. Kessel, J. Korbelik, J. Moan and Q. Peng (1998) Photodynamic therapy. *J. Natl Cancer Inst.* **90**, 889–905.
17. Bonnett, R. (2000) *Chemical Aspects of Photodynamic Therapy*. Gordon and Breach, Amsterdam.
18. Anderson, R. R. and J. A. Parrish (1981) The optics of human skin. *J. Invest. Dermatol.* **77**, 13–19.
19. Jonker, J. W., S. Musters, M. L. Vlaming, T. Plosch, K. E. Gooijert, M. J. Hillebrand, H. Rosing, J. H. Beijnen, H. J. Verkade and A. H. Schinkel (2007) Breast cancer resistance protein (Bcrp1/Abcg2) is expressed in the harderian gland and mediates transport of conjugated protoporphyrin IX. *Am. J. Physiol. Cell Physiol.* **292**, C2204–C2212.
20. Jonker, J. W., M. Buitelaar, E. Wagenaar, M. A. Van der Valk, G. L. Scheffer, R. J. Scheper, T. Plosch, F. Kuipers, R. P. J. O. Elferink, H. Rosing, J. H. Beijnen and A. H. Schinkel (2002) The breast cancer resistance protein protects against a major chlorophyll-derived dietary phototoxin and protoporphyria. *Proc. Natl Acad. Sci. USA* **99**, 15649–15654.
21. Bonnett, R. and G. Martinez (2001) Photobleaching of sensitizers used in photodynamic therapy. *Tetrahedron* **57**, 9513–9547.

22. Limantara, L., P. Koehler, B. Wilhelm, R. J. Porra and H. Scheer (2006) Photostability of bacteriochlorophyll *a* and derivatives. *Photochem. Photobiol.* **82**, 770–780.
23. Fiedor, J., L. Fiedor, N. Kammhuber, A. Scherz and H. Scheer (2002) Photodynamics of the bacteriochlorophyll-carotenoid system. 2. Influence of central metal, solvent and β-carotene on photobleaching of bacteriochlorophyll derivatives. *Photochem. Photobiol.* **76**, 145–152.
24. Kräutler, B. and S. Hörtensteiner (2006) Chlorophyll catabolites and the biochemistry of chlorophyll breakdown. In *Chlorophylls and Bacteriochlorophylls: Biochemistry, Biophysics, Functions and Applications* (Edited by B. Grimm, R. Porra, W. Rüdiger and H. Scheer), pp. 237–260. Springer, Dordrecht.
25. Ortiz de Montellano, P. R. and K. Auclair (2002) Heme oxygenase structure and mechanism. In *The Porphyrin Handbook. Vol. 12, The Iron and Cobalt Pigments: Biosynthesis, Structure, Degradation* (Edited by K. M. Kadish, K. M. Smith and R. Guilard), pp. 183–210. Academic Press, Amsterdam.
26. Dougherty, T. J. (1987) Photosensitizers: Therapy and detection of malignant tumors. *Photochem. Photobiol.* **45**, 879–889.
27. Posen, Y., V. Kalchenko, R. Seger, A. Brandis, A. Scherz and Y. Salomon (2005) Manipulation of redox signaling in mammalian cells enabled by controlled photogeneration of reactive oxygen species. *J. Cell Sci.* **118**, 1957–1969.
28. Kessel, D., M. G. H. Vicente and J. J. J. Reiners (2006) Initiation of apoptosis and autophagy by photodynamic therapy. *Autophagy* **2**, 289–290.
29. Plaetzer, K., T. Kiesslich, C. B. Oberdanner and B. Krammer (2005) Apoptosis following photodynamic tumor therapy: Induction, mechanisms and detection. *Curr. Pharm. Design* **11**, 1151–1165.
30. Piette, J., C. Volanti, A. Vantieghem, J.-Y. Matroule, Y. Habraken and P. Agostinis (2003) Cell death and growth arrest in response to photodynamic therapy with membrane-bound photosensitizers. *Biochem. Pharmacol.* **66**, 1651–1659.
31. Oleinick, N. L., R. L. Morris and I. Belichenko (2002) The role of apoptosis in response to photodynamic therapy: What, where, why, and how. *Photochem. Photobiol. Sci.* **1**, 1–21.
32. Moor, A. C. E. (2000) Signaling pathways in cell death and survival after photodynamic therapy. *J. Photochem. Photobiol. B, Biol.* **57**, 1–13.
33. Henderson, B. W. and T. J. Dougherty (1992) How does photodynamic therapy work? *Photochem. Photobiol.* **55**, 145–157.
34. Mazor, O., A. Brandis, V. Plaks, E. Neumark, V. Rosenbach-Belkin, Y. Salomon and A. Scherz (2005) WST11, a novel water-soluble bacteriochlorophyll derivative; cellular uptake, pharmacokinetics, biodistribution and vascular-targeted photodynamic activity using melanoma tumors as a model. *Photochem. Photobiol.* **81**, 342–351.
35. Brandis, A., O. Mazor, E. Neumark, V. Rosenbach-Belkin, Y. Salomon and A. Scherz (2005) Novel water-soluble bacteriochlorophyll derivatives for vascular-targeted photodynamic therapy: Synthesis, solubility, phototoxicity and the effect of serum proteins. *Photochem. Photobiol.* **81**, 983–993.
36. Vakrat-Haglili, Y., L. Weiner, V. Brumfeld, A. Brandis, Y. Salomon, B. McIlroy, B. C. Wilson, A. Pawlak, M. Rozanowska, T. Sarna and A. Scherz (2005) The microenvironment effect on the generation of reactive oxygen species by Pd-bacteriopheophorbide. *J. Am. Chem. Soc.* **127**, 6487–6497.
37. Ashur, I., R. Goldschmidt, I. Pinkas, Y. Salomon, G. Szewczyk, T. Sarna and A. Scherz (2009) Photocatalytic generation of oxygen radicals by the water-soluble bacteriochlorophyll derivative WST11, noncovalently bound to serum albumin. *J. Phys. Chem.* **113**, 8827–8837.
38. Lindsay Smith, J. R. and M. Calvin (1966) Chemical and photochemical oxidation of bacteriochlorophyll. *J. Am. Chem. Soc.* **88**, 4500–4506.
39. Struck, A., E. Cmiel, I. Katheder, W. Schaefer and H. Scheer (1992) Bacteriochlorophylls modified at position C-3: Long-range intramolecular interaction with position C-13^2. *Biochim. Biophys. Acta* **1101**, 321–328.
40. Omata, T. and N. Murata (1986) A rapid and efficient method to prepare chlorophyll *a* and *b* from leaves. *Photochem. Photobiol.* **31**, 183–185.
41. Benedetti, C. E. and P. Arruda (2002) Altering the expression of the chlorophyllase gene *ATHCOR1* in transgenic *Arabidopsis* caused changes in the chlorophyll-to-chlorophyllide ratio. *Plant Physiol.* **128**, 1255–1263.
42. Hynninen, P. H. (1991) Chemistry of chlorophylls: Modifications. In *Chlorophylls* (Edited by H. Scheer), pp. 145–210. CRC Press, Boca Raton, FL.
43. Helfrich, M., S. Schoch, U. Lempert, E. Cmiel and W. Rüdiger (1994) Chlorophyll synthetase cannot synthesize chlorophyll *a*′. *Eur. J. Biochem.* **219**, 267–275.
44. Strell, M. and T. Urumow (1977) New methods for introduction of metals into derivatives of chlorophyll. *Justus Liebigs Ann. Chem.*, 970–974.
45. Hartwich, G., L. Fiedor, I. Simonin, E. Cmiel, W. Schaefer, D. Noy, A. Scherz and H. Scheer (1998) Metal-substituted bacteriochlorophylls. 1. Preparation and influence of metal and coordination on spectra. *J. Am. Chem. Soc.* **120**, 3675–3683.
46. Havel, R. J., H. A. Eder and J. H. Bragdon (1955) Distribution and chemical composition of ultracentrifugally separated lipoproteins in human serum. *J. Clin. Invest.* **34**, 1345–1353.
47. Graham, J. (2001) *Biological Centrifugation.* BIOS Scientific Publishers, Oxford.
48. Whitacre, C. M., D. K. Feyes, T. Satoh, J. Grossmann, J. W. Mulvihill, H. Mukhtar and N. L. Oleinick (2000) Photodynamic therapy with the phthalocyanine photosensitizer Pc 4 of SW480 human colon cancer xenografts in athymic mice. *Clin. Cancer Res.* **6**, 2021–2027.
49. Graham, J. M., J. A. Higgins, T. Gillott, T. Taylor, J. Wilkinson, T. Ford and D. Billington (1996) A novel method for the rapid separation of plasma lipoproteins using self-generating gradients of iodixanol. *Atherosclerosis* **124**, 125–135.
50. Noy, D., L. Fiedor, G. Hartwich, H. Scheer and A. Scherz (1998) Metal-substituted bacteriochlorophylls. 2. Changes in redox potentials and electronic transition energies are dominated by intramolecular electrostatic interactions. *J. Am. Chem. Soc.* **120**, 3684–3693.
51. Buchler, J. W. (1975) Static coordination chemistry of metalloporphyrins. In *Porphyrins and Metalloporphyrins* (Edited by K. M. Smith), pp. 157–232. Elsevier, Amsterdam.
52. Scheer, H. (2006) Overview. In *Chlorophylls and Bacteriochlorophylls: Biochemistry, Biophysics, Functions and Applications* (Edited by B. Grimm, R. Porra, W. Rüdiger and H. Scheer), pp. 1–26. Springer, Dordrecht.
53. Watanabe, T. and M. Kobayashi (1991) Electrochemistry of chlorophylls. In *Chlorophylls* (Edited by H. Scheer), pp. 287–316. CRC Press, Boca Raton, FL.
54. Madörin, M., P. van Hoogevest, R. Hilfiker, B. Langwost, G. M. Kresbach, M. Ehrat and H. Leuenberger (1997) Analysis of drug/plasma protein interactions by means of asymmetrical flow field-flow fractionation. *Pharm. Res.* **14**, 1706–1712.
55. Davies, I. G., J. M. Graham and B. A. Griffin (2003) Rapid separation of LDL subclasses by iodixanol gradient ultracentrifugation. *Clin. Chem.* **49**, 1865–1872.
56. Reyftmann, J. P., P. Morliere, S. Goldstein, R. Santus, L. Dubertret and D. Lagrange (1984) Interaction of human serum low density lipoproteins with porphyrins: A spectroscopic and photochemical study. *Photochem. Photobiol.* **40**, 721–729.
57. Jori, G., M. Beltramini, E. Reddi, B. Salvato, A. Pagnan, L. Ziron, L. Tomio and T. Tsanov (1984) Evidence for a major role of plasma lipoproteins as hematoporphyrin carriers *in vivo*. *Cancer Lett.* **24**, 291–297.
58. Jori, G. and E. Reddi (1993) The role of lipoproteins in the delivery of tumour-targeting photosensitizers. *Int. J. Biochem.* **25**, 1369–1375.
59. Hoebeke, M. (2000) ESR associated to spin label method in the study of photosensitization in liposomal solution. *Bull. Soc. Roy. Sci. Liege* **69**, 103–110.
60. Kostner, G. M. and W. März (2001) Zusammensetzung und Stoffwechsel der Lipoproteine. In *Handbuch Der Fettstoffwech selstörungen* (Edited by P. Schwandt, W. O. Richter and K. G. Parhofer), pp. 1–57. Schaffauer, Stuttgart.
61. Szczygiel, M., K. Urbanska, P. Jurecka, I. Stawoska, G. Stochel and L. Fiedor (2008) Central metal determines pharmacokinetics of chlorophyll-derived xenobiotics. *J. Med. Chem.* **51**, 4412–4418.

62. Yerushalmi, R., I. Ashur and A. Scherz (2006) Metal-substituted bacteriochlorophylls: Novel molecular tools. In *Chlorophylls and Bacteriochlorophylls: Biochemistry, Biophysics, Functions and Applications* (Edited by B. Grimm, R. Porra, W. Rüdiger and H. Scheer), pp. 495–506. Springer, Dordrecht.
63. Evans, T. A. and J. J. Katz (1975) Evidence for 5 and 6-coordinated magnesium in bacteriochlorophyll *a* from visible absorption spectroscopy. *Biochim. Biophys. Acta* **396**, 414–426.
64. Noy, D., R. Yerushalmi, V. Brumfeld, I. Ashur, H. Scheer, K. K. Baldridge and A. Scherz (2000) Optical absorption and computational studies of [Ni]-bacteriochlorophyll *a*. New insight into charge distribution between metal and ligands. *J. Am. Chem. Soc.* **122**, 3937–3944.
65. Haehnel, W., D. Noy and H. Scheer (2008) *De novo* designed bacteriochlorophyll-binding helix-bundle proteins. In *The Purple Phototrophic Bacteria* (Edited by C. N. Hunter, F. Daldal, M. C. Thurnauer and J. T. Beatty), pp. 895–912. Springer, Dordrecht.
66. Fiedor, L. (2006) Hexacoordination of bacteriochlorophyll in photosynthetic antenna LH1. *Biochemistry* **45**, 1910–1918.
67. Bröring, M. and C. D. Brandt (2003) A five coordinate Pd(II) complex stable in solution and in the solid state. *Chem. Commun.*, 2156–2157.
68. Cotton, T. M., P. A. Loach, J. J. Katz and K. H. Ballschmiter (1976) Studies of chlorophyll–chlorophyll and chlorophyll–ligand interactions. *Photochem. Photobiol.* **27**, 735.
69. Kania, A. and L. Fiedor (2006) Steric control of bacteriochlorophyll ligation. *J. Am. Chem. Soc.* **128**, 454–456.
70. Scheer, H. and J. J. Katz (1974) Structure of the Krasnovskii photoreduction product of chlorophyll *a*. *Proc. Natl Acad. Sci. USA* **71**, 1626–1629.
71. Scheer, H. (1988) Chlorophylls: Chromatographic methods for the separation of chlorophylls. In *Chlorophylls* (Edited by H.-P. Köst), pp. 235–307. CRC Press, Boca Raton.
72. Beltramini, M., P. A. Firey, F. Ricchelli, M. A. J. Rodgers and G. Jori (1987) Steady-state and time-resolved spectroscopic studies on the hematoporphyrin-lipoprotein complex. *Biochemistry* **26**, 6852–6858.
73. Kepczynski, M., R. P. Pandian, K. M. Smith and B. Ehrenberg (2002) Do liposome-binding constants of porphyrins correlate with their measured and predicted partitioning between octanol and water? *Photochem. Photobiol.* **76**, 127–134.
74. Garbo, G. M. (1990) The use of liposomes, emulsions or inclusion complexes may potentiate *in vivo* effects of SnET2. *Proc. SPIE* **1203**, 118–125.
75. Kessel, D., A. Morgan and G. M. Garbo (1991) Sites and efficacy of photodamage by tin Etiopurpurin *in vitro* using different delivery systems. *Photochem. Photobiol.* **54**, 193–196.
76. Polo, L., E. Reddi, G. M. Garbo, A. R. Morgan and G. Jori (1992) The distribution of the tumor photosensitizers zinc(II)-phthalocyanine and tin (IV)-etiopurpurin among rabbit plasma proteins. *Cancer Lett.* **66**, 217–223.
77. Kongshaug, M., J. Moan, L. S. Cheng, G. M. Garbo, S. Kolboe, A. R. Morgan and C. Rimington (1993) Binding of drugs to human plasma proteins, exemplified by tin(IV)-etiopurpurin dichloride delivered in Cremophor and DMSO. *Int. J. Biochem.* **25**, 739–760.
78. Kongshaug, M., L. S. Cheng, J. Moan and C. Rimington (1991) Interaction of Cremophor EL with human plasma. *Int. J. Biochem.* **23**, 473–478.
79. Woodburn, K. and D. Kessel (1994) The alteration of plasma lipoproteins by Cremophor EL. *J. Photochem. Photobiol. B, Biol.* **22**, 197–201.
80. Griffin, B. A., M. J. Caslake, B. Yip, G. W. Tait, C. J. Packard and J. Shepherd (1990) Rapid isolation of low density lipoprotein (LDL) subfractions from plasma by density gradient ultracentrifugation. *Atherosclerosis* **83**, 59–67.
81. Jacob, S. W. and R. Herschler (1986) Pharmacology of DMSO. *Cryobiology* **23**, 14–27.
82. Santos, N. C., J. Figueira-Coelho, J. Martins-Silva and C. Saldanha (2003) Multidisciplinary utilization of dimethyl sulfoxide: Pharmacological, cellular, and molecular aspects. *Biochem. Pharmacol.* **65**, 1035–1041.
83. Webster, L. K., D. M. Woodcock, D. Rischin and M. J. Millward (1997) Cremophor: Pharmacological activity of an ''inert'' solubilizer. *J. Oncol. Pharm. Pract.* **3**, 186–192.
84. Haylett, A. K. and J. V. Moore (2002) Comparative analysis of fetal calf and human low density lipoprotein: Relevance for pharmacodynamics of photosensitizers. *J. Photochem. Photobiol. B, Biol.* **66**, 171–178.
85. Cunderlikova, B., M. Kongshaug, L. Gangeskar and J. Moan (2000) Increased binding of chlorin e_6 to lipoproteins at low pH values. *Int. J. Biochem. Cell Biol.* **32**, 759–768.
86. Hopkinson, H. J., D. I. Vernon and S. B. Brown (1999) Identification and partial characterization of an unusual distribution of the photosensitizer meta-tetrahydroxyphenyl chlorin (temoporfin) in human plasma. *Photochem. Photobiol.* **69**, 482–488.
87. Trachtenberg, J., R. A. Weersink, S. R. H. Davidson, M. A. Haider, A. Bogaards, M. R. Gertner, A. Evans, A. Scherz, J. Savard, J. L. Chin, B. C. Wilson and M. Elhilali (2008) Vascular-targeted photodynamic therapy (padoporfin, WST09) for recurrent prostate cancer after failure of external beam radiotherapy: A study of escalating light doses. *BJU Int* **102**, 556–562.
88. Kongshaug, M., J. Moan and S. B. Brown (1989) The distribution of porphyrins with different tumor localizing ability among human plasma proteins. *Br. J. Cancer* **59**, 184–188.
89. Kessel, D., P. Thompson, K. Saatio and K. D. Nantwi (1987) Tumor localization and photosensitization by sulfonated derivatives of tetraphenylporphine. *Photochem. Photobiol.* **45**, 787–790.
90. Woodburn, K. and D. Kessel (1995) Effect of density-gradients on the binding of photosensitizing agents to plasma proteins. *Int. J. Biochem. Cell Biol.* **27**, 499–506.
91. Vilensky, J., N. V. Koudinova, A. Harmelin, A. Scherz and Y. Salomon (2005) Vascular-targeted photodynamic therapy (VTP) of a canine-transmissible venereal tumour in a murine model with Pd-bacteriopheophorbide (WST09). *Vet. Comp. Oncol.* **3**, 182–193.
92. Koudinova, N. V., J. H. Pinthus, A. Brandis, O. Brenner, P. Bendel, J. Ramon, Z. Eshhar, A. Scherz and Y. Salomon (2003) Photodynamic therapy with Pd-bacteriopheophorbide (TOOKAD): Successful *in vivo* treatment of human prostatic small cell carcinoma xenografts. *Int. J. Cancer* **104**, 782–789.
93. Kessel, D. and K. Woodburn (1993) Biodistribution of photosensitizing agents. *Int. J. Biochem.* **25**, 1377–1383.
94. Polo, L., G. Bianco, E. Reddi and G. Jori (1995) The effect of different liposomal formulations on the interaction of Zn(II)-phthalocyanine with isolated low and high density lipoproteins. *Int. J. Biochem. Cell Biol.* **27**, 1249–1255.
95. Tyssandier, V., G. Choubert, P. Grolier and P. Borel (2002) Carotenoids, mostly the xanthophylls, exchange between plasma lipoproteins. *Int. J. Vitam. Nutr. Res.* **72**, 300–308.
96. Moss, G. P. (1988) IUPAC-IUB Joint Commission Biochemical Nomenclature (JCBN). Nomenclature of Tetrapyrroles. Recommendation 1986. *Eur. J. Biochem.* **178**, 277–328.